Designing Comb-Chain Crosslinker-Based Solid Polymer Electrolytes for Additive-Free All-Solid-State Lithium Metal Batteries

Xiaowei Li,[†] *Yongwei Zheng,*[†] *Yipin Duan,*[†] *Mingwei Shang,*[‡] *Junjie Niu*[‡] *and Christopher Y. Li**[†]

[†] Department of Materials Science and Engineering, Drexel University, Philadelphia, PA 19104, USA

[‡] Department of Materials Science and Engineering, University of Wisconsin-Milwaukee, Milwaukee, WI 53211, USA

KEYWORDS: solid polymer electrolytes, network solid polymer electrolytes, lithium metal batteries, lithium dendrite

ABSTRACT: Developing solid polymer electrolytes (SPEs) is a promising approach to realize practical dendrite-free lithium metal batteries (LMBs). Tuning the nanoscale polymer network chemsitry is of critical importance for SPE design. In this work, we take lessons from the rubber chemistry and develop a series of comb-chain crosslinker-based SPEs (ConSPEs) using a preformed polymer as the multifunctional crosslinker. The high-functionality cross-linker

increases the connectivity of nanosized cross-linked domains, which leads to a robust network with dramatically improved toughness and superior lithium dendrite resistance even at a current density of 2 mA cm^{-2}. The uniform and flexile network also dramatically improves the anodic stability to over 5.3 V vs. Li/Li^{+}. Additive-free, all-solid-state LMBs with the ConSPE show high discharge capacity and stable cycling up to 10 C rate, and can be stably cycled at 25 °C. Our results show that ConSPEs are promising for high-performance and dendrite-free LMBs.

Lithium metal batteries (LMBs) with lithium metal as the anode are regarded as the next-generation energy storage system due to their high energy density, while the practical application is hindered by the active lithium metal/electrolytes reaction and the associated morphology including lithium dendrites and orphaned lithium metal at the electrode/electrolytes interface during long cycling.[1-6] Utilizing solid polymer electrolytes (SPEs) to replace the commonly used liquid electrolytes has been proved to be an effective way to suppress the lithium dendrite growth.[2, 7, 8] Compared with liquid electrolytes, some of the crucial advantages of SPEs include leak-free, high thermal stability, flexibility, and good processability.[2, 7-11] Tremendous efforts have been devoted to developing numerous advanced SPE systems while their lithium dendrite resistance at high current densities still needs to be further improved to render SPEs a practical choice for future LMBs.

Based on their chain architecture, reported SPEs can be divided into five categories, *i.e.* main-chain, side-chain, block copolymer, multiblock copolymer, and network SPEs.[12-22] Studies have shown that all these architectures can be used to tune mechanical properties and ionic conductivity of the SPEs. However, symmetrical lithium cell cycling tests demonstrated that the classical main-chain, side-chain, and block copolymer SPEs suffer from poor lithium dendrite resistance, which can be attributed to their limited physical chain entanglements and that these SPEs are susceptible to plastically deform at large strain. On the other hand, network SPEs, although with a moderate shear modulus, perform the best in reported device tests,[2, 7, 23-25] which suggests that the permanent chemical crosslinking in the network SPEs mitigates potential chain disentanglement induced by the large volume change of the electrodes during cycling and creeping, leading to enhanced device performance.

Multi-functional monomers (functionality f ≥3) are typically introduced to a reaction system to form a chemically crosslinked network following either an addition chain polymerization or a step-growth polymerization mechanism.[26, 27] For additional chain polymerization, polyethylene-poly (ethylene oxide) (PEO)-based SPEs were synthesized using ring-opening metathesis polymerization followed by hydrogenation.[24] Photopolymerization of acrylate-terminated PEO to form solid or gel SPEs have been reported.[7, 25, 28] For step-growth polymerization, epoxide-bearing polyhedral oligomeric silsesquioxane (POSS) crosslinkers have been used to crosslink diamine poly(ethylene glycol) (PEG) using a one-pot, single step polymerization procedure.[18, 29-32] In all these SPEs, small crosslinked domains firstly grow and then connect to form the network. Inevitably there can be heterogeneity as the isolated cross-linked domains grow and merge into a macroscopic network (**Scheme 1a**). The typically small molecular mesh size associated with this method also leads to a relatively rigid network system. Designing an SPE to accommodate large volume change, therefore, calls for a highly deformable and elastic polymer system.

Another method to form network structure is crosslinking pre-formed polymers, such as sulfur vulcanization of natural rubber.[26, 27] The preformed polymer ensures controlled viscosity and a uniform network structure with a large design space to tune the mesh size, elasticity, and toughness of the material as demonstrated in highly elastic and deformable polymer rubbers. In this work, following the strategy of rubber chemistry, we introduce a macromolecular crosslinker, poly (glycidyl methacrylate) (PGMA), with epoxy side groups to form a series of ***co***mb-chain crosslinker-based ***n***etwork SPEs (ConSPEs). As shown in **Scheme 1b**, because of the comb-chain architecture, each polymer has many epoxide functional groups for the crosslinking reaction — for a molar mass of 15,000 g mol^{-1} PGMA, 106 epoxide groups are available for further crosslinking/functionalization! These groups can easily react with the amine chain ends from PEG. Due to the large number of functional groups, gelation occurs much earlier in ConSPEs compared with previous reported network SPEs. According to the gelation theory, the critical branching coefficient $\alpha_c = \frac{1}{f-1}$, where f is the functionality, 8 for the previously reported POSS network SPE and 106 for the PGMA comb-chain crosslinker.[18] α_c for these two networks are therefore 0.14 and 0.0095, respectively. This dramatic α_c difference suggests that it is much easier to gel in a ConSPE, leading to a fixed homogeneous morphology. Furthermore, the enhanced initial viscosity and retarded diffusion kinetics associated with the large molar mass of comb-chain crosslinker delay phase separation and a homogeneous phase will be more readily obtained in the ConSPEs. Meanwhile, the flexibility of the PGMA chains further enhances the toughness of the ConSPE membranes.

In this work, PGMA-based ConSPEs are synthesized using a facile one-pot method. The chemical, thermal, mechanical, and electrochemical properties of the ConSPEs are carefully characterized. The correlation between the network structure and ConSPE performance is thoroughly researched by preparing a series of ConSPEs with different crosslinking densities and network mesh sizes through changing the PGMA monomer/PEG molar ratio and PEG molar mass, respectively. The prepared PGMA-PEG ConSPEs exhibit superior overall properties and improved LMB device performance compared with the state-of-the-art SPEs with an ionic conductivity of 1.31×10^{-4} S cm^{-1} at 40 °C, high electrochemical stability over 5.3 V vs. Li/Li^+, excellent toughness, excellent lithium dendrite resistance up to 2 mA cm^{-2}, and superior battery performance at a wide temperature range from 25 °C to 90 °C.

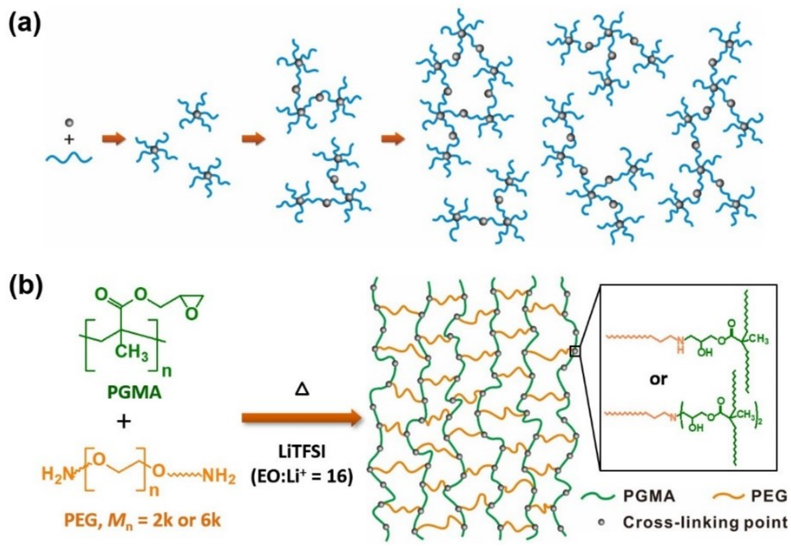

Scheme 1. Schematics of network formation. (a) Network formed from small molar mass crosslinker (gray dots); (b) Network formed by a comb-chain crosslinker.

As shown in **Scheme 1**, the homogeneously crosslinked network of PGMA-PEG ConSPEs (denoted as *x*PGMA-PEG*n*, in which *x* denotes the molar ratio of PGMA monomer/PEG, and *n* is the PEG molar mass, as shown in **Table 1**) was formed by the reaction between epoxy groups from PGMA and amine groups from amine-terminated PEG. Lithium bis(trifluoromethanesulfonyl)imide (LiTFSI) (molar ratio of $EO/Li^+ = 16$) with high ionic conductivity and thermal stability[9] was employed as the lithium salt. The obtained ConSPE membranes are transparent and flexible, with a smooth surface as observed from photographs and scanning electron microscopy (SEM) image in **Figure S1**. Fourier transform infrared (FTIR) spectra (**Figure S2**) indicate that all the ConSPE samples are highly crosslinked since the majority of epoxy groups have reacted after crosslinking.

Thermal properties of the as-prepared PGMA-PEG ConSPEs were evaluated using differential scanning calorimetry (DSC) and thermal gravimetric analysis (TGA), and the results are shown in **Figure 1a** and **Figure S3**, respectively. The glass transition temperature, T_g, and the degree of crystallinity, X_c, of the ConSPE samples are listed in **Table 1**. T_g of PGMA homopolymer is 62 °C. For ConSPEs, due to the large PEG content, PEG dominates the system. The ConSPE T_gs range from -47.2 to -39.1 °C and it decreases with the EO content in the network. There is no PEG crystallization peak for the two ConSPE samples with PEG2k, indicating that the PEG crystallization was completely suppressed after crosslinking. For ConSPEs with PEG6k, DSC heating curves show a recrystallization exothermic peak before crystal melting. The endothermic melting peaks are located between 32 °C and 33 °C, which are much lower than the melting temperatures of PEG2k and PEG6k homopolymers, suggesting poor crystalline structure in the ConSPEs. The degree of crystallinity X_c of ConSPE samples can be calculated from the equation

$$X_c = (\Delta H_m - \Delta H_c)/(\Delta H_{m,0} \times w) \quad (1)$$

in which ΔH_m, ΔH_c, $\Delta H_{m,0}$ and w denote the ConSPE melting enthalpy, enthalpy of recrystallization, the melting enthalpy of a 100% crystalline form of PEO (196.6 J g^{-1}),[33] and the PEG weight percentage in the ConSPE, respectively. Relatively low X_cs of 14.5% and 15.6% are found for these two ConSPEs as shown in Table 1, suggesting that a small portion of the PEG is crystallized in the sample. From the TGA curves shown in **Figure S3**, it can be seen that thermal decomposition temperatures $T_{5\%}$ (temperature when 5% weight loss occurs) for the PGMA-PEG ConSPEs are between 325 °C and 351 °C, confirming its high thermal stability, which is crucial for high temperature applications as well as mitigating the safety hazard triggered by thermal runaway.[34]

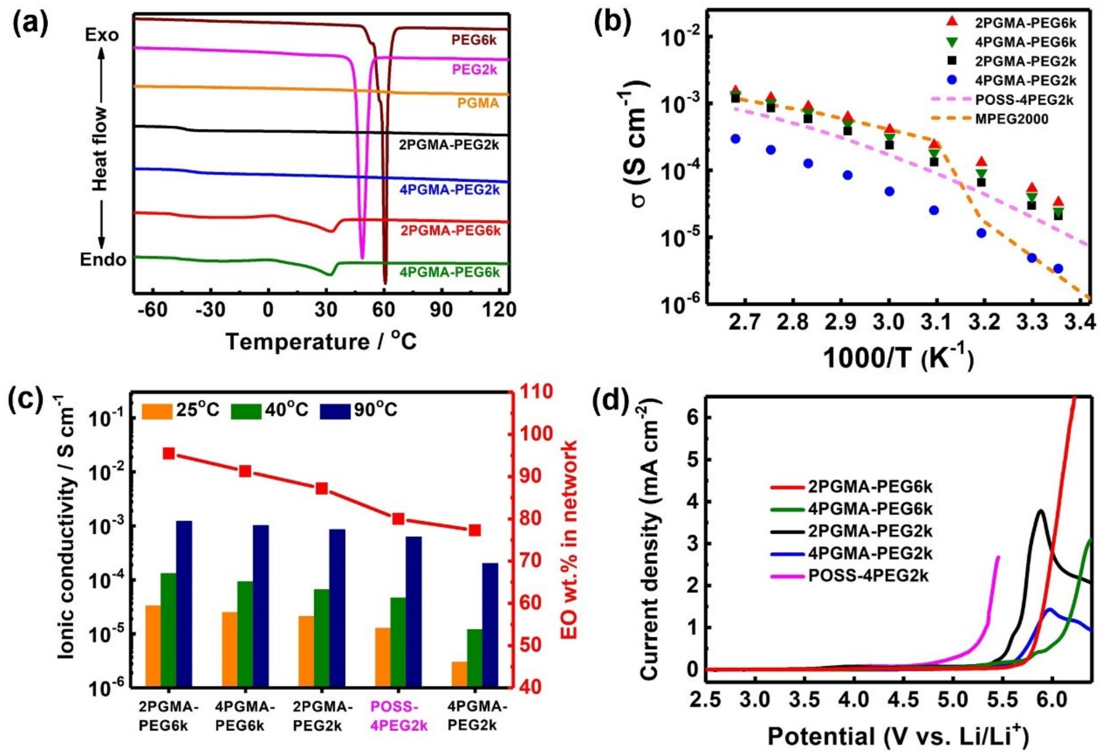

Figure 1. Thermal and electrochemical properties of PGMA-PEG ConSPEs: (a) DSC second heating thermograms; (b) temperature dependence of ionic conductivities (ionic conductivities of POSS-4PEG2k and MPEG2000 are from Ref. [30] and [35], respectively); (c) comparison of ionic conductivities at 25 °C, 40 °C and 90 °C, and EO weight ratio in the network; and (d) LSV curves (LSV curve of POSS-4PEG2k is from Ref. [30]).

Table 1. Characteristics of PGMA-PEG ConSPEs.

ConSPE	EO wt/% in network	EO wt/% in ConSPE	T_g [°C]	X_c [%]	Ionic conductivity [mS cm^{-1}]			Oxidation potential [V]	t_{Li+}
					25 °C	40 °C	90 °C		
2PGMA-PEG2k	87.2	64.3	-42.9	–	0.021	0.066	0.854	5.3	0.188
4PGMA-PEG2k	77.3	58.6	-39.1	–	0.003	0.012	0.203	5.5	0.150
2PGMA-PEG6k	95.5	68.7	-47.2	15.6	0.033	0.131	1.22	5.5	0.234
4PGMA-PEG6k	91.3	66.6	-46.0	14.5	0.025	0.092	1.02	5.7	0.172

Ionic conductivities of PGMA-PEG ConSPEs were measured using AC impedance spectroscopy. **Figure 1b** and **Table 1** show that the ionic conductivities increase with temperature, and the curves can be fitted with the Vogel−Tammann−Fulcher (VTF) equation (**Figure S4**, **Table S1**), demonstrating that the ion transport in PGMA-PEG ConSPEs is facilitated by polymer chain reptation.[36] EO weight ratio in the network and ionic conductivities at 25 °C, 40 °C and 90 °C for the ConSPEs are listed and plotted in **Table 1** and **Figure 1c**. For all the ConSPE samples, with the increase of EO weight ratio in the network, the ionic conductivity increases and the activation energy decreases, which is because PEG acts as the lithium ion solvating medium, and increasing the PEG content could decrease T_g and also increase the number of dissociated ions since the EO/Li molar ratio remains constant. Among all the ConSPEs, 2PGMA-PEG6k shows the highest ionic conductivity of 1.31×10^{-4} S cm^{-1} at 40 °C and 1.22×10^{-3} S cm^{-1} at 90 °C, which are comparable to the state-of-the-art all-solid-state SPEs,[18, 24] composite[37, 38] and plasticized[25, 39] polymer electrolytes. Compared with poly(ethylene glycol) methyl ether (MPEG, M_n = 2k)-LiTFSI SPE,[35] PGMA-PEG ConSPEs show similar ionic conductivities at high temperature (≥ 50 °C) and one order of magnitude higher below 40 °C, which is due to the suppression of PEG crystallization as confirmed by DSC results. Moreover, ionic conductivities of the previously reported POSS-4PEG2k SPE[18, 30] are plotted in **Figures 1b,c** for comparison. The 2PGMA-PEG2k ConSPE with the same epoxy/amine ratio and PEG molar mass exhibits 1.3-1.8 times higher ionic conductivities than POSS-4PEG2k, which can be attributed to the higher EO weight ratio in the network (87.2% *vs.* 80.0% for POSS-4PEG2k).

The electrochemical stability is evaluated by linear sweep voltammetry (LSV). As shown in **Figure 1d** and **Table 1**, compared with linear PEO-based SPEs and POSS-4PEG2k SPE (4-4.5 V),[30, 40] the anodic stability of the ConSPEs dramatically enhances to over 5.3 V vs. Li/Li^+, and increases with the increase of PGMA content, which could be attributed to the robust cross-linking network structure and the ester groups in PGMA that act as a protective layer for EO groups.[41] The higher anodic stability of ConSPEs with PEG6k compared to those with PEG2k is likely due to less terminal groups that are unstable at high voltage.[42] The remarkable electrochemical stability enables the combination of ConSPEs with high-voltage cathodes ($LiNi_xMn_yCo_{1-x-y}O_2$, $LiCoO_2$, et al.) for high-energy-density LMBs. The lithium ion transference numbers t_{Li+} of PGMA-PEG ConSPEs are between 0.150 and 0.234 (**Figure S5**, **Table 1**), which are typical for PEO-based SPEs.[8, 18, 43]

Sufficient mechanical strength is essential for successful battery applications and lithium dendrite growth resistance[44] during repeated cycling in LMBs. The mechanical properties of PGMA-PEG ConSPEs were investigated by tensile tests at both 25 °C and 90 °C, and the results are shown in **Figure 2** and **Table S2**. For ConSPEs with PEG2k, there is no significant change from 25 °C to 90 °C since PEG crystallization is completely suppressed. While for ConSPEs with

PEG6k, due to partial crystallization of PEG, the modulus and toughness decrease when the temperature rises to 90 °C. When increasing the PEG molar mass from 2k to 6k g mol^{-1}, ConSPE modulus decreases while its elongation-at-break and toughness significantly increase. 4PGMA-PEG6k ConSPE shows the highest toughness at both 25 °C and 90 °C. The mechanical properties of the POSS-PEG SPE are also listed in **Table S2** for comparison. The toughness of 2PGMA-PEG2k ConSPE is 5.6 times that of the POSS-4PEG2k SPE with the same epoxy/amine ratio and PEG molar mass, which confirms our strategy that employing high-functionality PGMA as the cross-linker would generate a more robust network.

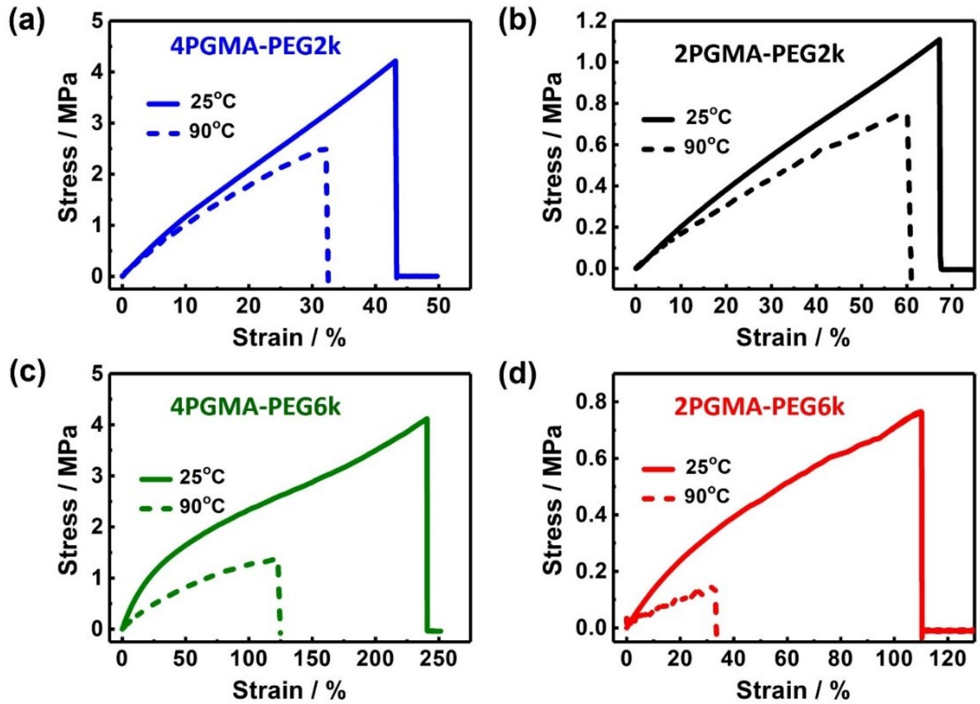

Figure 2. Stress-strain curves for (a) 4PGMA-PEG2k, (b) 2PGMA-PEG2k, (c) 4PGMA-PEG6k, and (d) 2PGMA-PEG6k at 25 °C and 90 °C.

Lithium plating-stripping tests were employed to evaluate the lithium deposition stability and the lithium dendrite resistance of the PGMA-PEG ConSPEs. As shown in **Figure 3**, symmetrical lithium cells with the 4PGMA-PEG6k ConSPE exhibits a short circuit time t_{sc} of 580 h when cycled at 90 °C under the current density of 1 mA cm^{-2} with an areal capacity of 3 mAh cm^{-2}, and 266 h under 2 mA cm^{-2} with 2 mAh cm^{-2}. Even at 25 °C, the cell is able to deliver stable cycling under the current density of 0.05 mA cm^{-2} with the areal capacity of 0.05 mAh cm^{-2} for over 6000 h, indicating high stability with lithium and excellent lithium dendrite resistance of the ConSPE. **Figure S6** shows the time-voltage profiles for the other three ConSPEs. All samples exhibit stable lithium plating-stripping behavior over 100 h at 90 °C under 1 mA cm^{-2} with the areal capacity of up to 3 mAh cm^{-2}. In the previous study, t_{sc} is proved to be proportional to the SPE thickness.[45] Therefore, the t_{sc} values from previous literatures and in this work are normalized using a thickness of 100 μm as the benchmark. While plotting normalized t_{sc} versus ConSPE modulus, a bell-shaped curve is seen in **Figure 3d**, indicating an optimum modulus for cell cycling, which is consistent with our previous report.[46] The plotting of normalized t_{sc} versus ConSPE toughness (**Figure 3d**) indicates that the normalized t_{sc} monotonically increases from 208 h to 315 h as the ConSPE toughness changed from 0.03 to 1.08 MJ m^{-3}. This confirms our hypothesis that rather than modulus, toughness which reflects both strength and extensibility[39] plays an important role in lithium dendrite resistance.

The short circuit time t_{sc} of ConSPEs is compared with the previously reported SPEs with different molecular architectures, as shown in **Figure 3e**. The 4PGMA-PEG6k ConSPE shows better performance than linear PEO SPEs,[47] copolymer SPEs[20, 48] and other cross-linked SPEs.[18, 24, 30, 32, 49] In particular, it demonstrates impressive performance at a high current density, which is desired for future LMB applications.

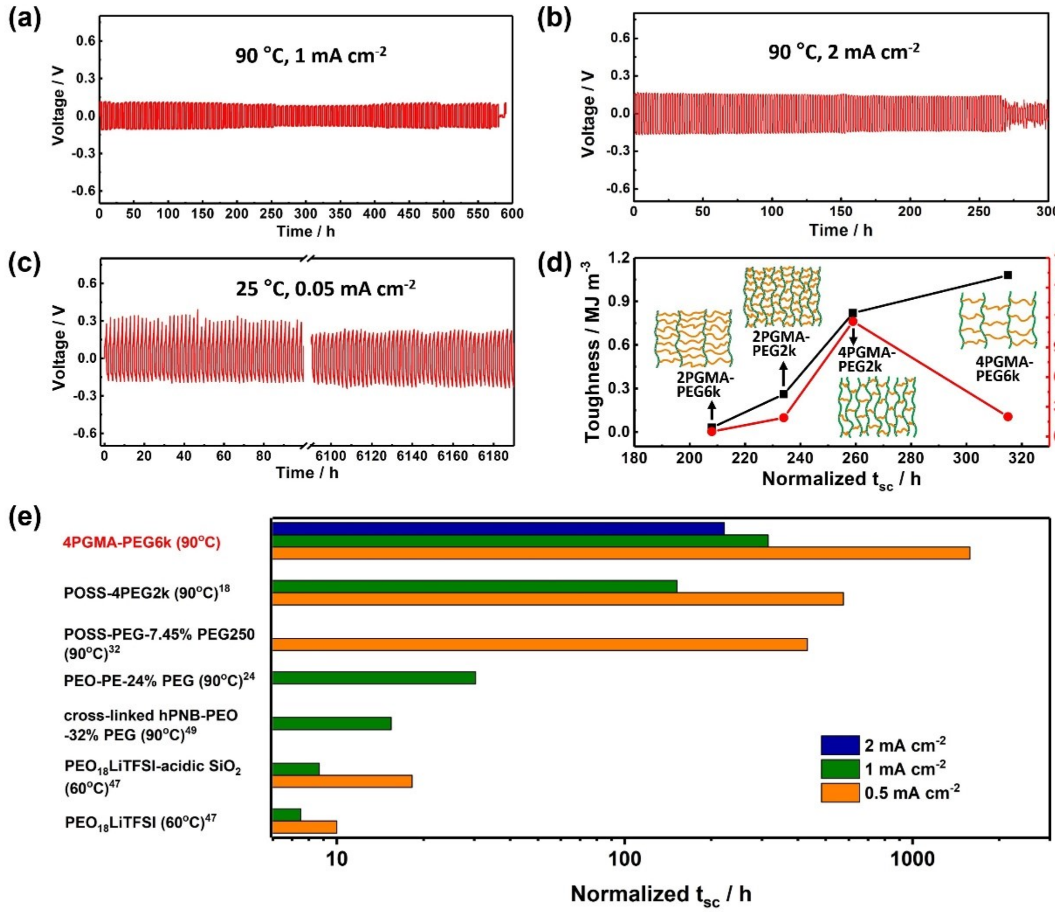

Figure 3. Time-voltage profiles of symmetrical lithium cells with the 4PGMA-PEG6k ConSPE (a) at 90 °C and 1 mA cm^{-2} with an areal capacity of 3 mAh cm^{-2}, (b) at 90 °C and 2 mA cm^{-2} with an areal capacity of 2 mAh cm^{-2}, and (c) at 25 °C and 0.05 mA cm^{-2} with an areal capacity of 0.05 mAh cm^{-2}. (d) Correlation of normalized short-circuit time t_{sc} for Li/ConSPE/Li cells (1 mA cm^{-2}, 3 mAh cm^{-2}, at least two cells were tested for each ConSPE and the average values were used) with ConSPE toughness and modulus. (e) Comparison of normalized short-circuit time t_{sc} for 4PGMA-PEG6k ConSPE developed in this work with the state-of-the-art SPEs.

The surface chemistry of lithium in the symmetrical Li/4PGMA-PEG6k/Li cell after cycling was examined by X-ray photoelectron spectroscopy (XPS), and the spectra for C 1s, O 1s, and F 1s are shown in **Figure S7**. The signals for N 1s and S 2p are too weak to be analyzed. The lithium surface contains similar components (C-C, C-OR, LiF, Li-OR, Li_2CO_3) to Li/PEO-LiTFSI SPE surface[50] with strong LiF and Li_2CO_3 signals and less salt degradation products (Li_2S, Li_2S_2, Li_2SO_3, Li_3N) compared to Li/POSS-PEG SPE surface,[46] which is attributed to the more integrated and robust PGMA-PEG network. Compared with the spectra before etching, the spectra after etching with Ar ion gun (1 kV for 1 min), which correspond to the inner SEI composition, show higher content of inorganic species LiF, LiOH and Li_2CO_3, and lower content of aliphatic carbon (C-C) and ether carbon (C-OR) from the polymer, exhibiting a construction similar to the mosaic-type SEI model.[51] COOR mainly derived from the decomposition of the ester group in PGMA also increases after etching, which may form a protective layer together with the inorganic species to protect the lithium anode and prevent the further decomposition of the lithium salts.

Since the 4PGMA-PEG6k ConSPE sample shows high ionic conductivity, good electrochemical stability, and outstanding mechanical strength, it was chosen for further LMB performance study. Because of the excellent mechanical toughness of the 4PGMA-PEG6k sample, an ultra-thin self-standing membrane with a thickness of about 20-30 μm was obtained. Thin SPEs are desired to improve the energy and power density of LMBs.[52] Since there is limited room for SPE conductivity improvement due to the chain reptation nature, thinner SPE membranes with lower SPE resistance can compensate for the relatively low SPE conductivity. Current ultrathin SPE membranes are obtained using a porous fiber scaffold infiltrated with polymer electrolytes.[52] In our ConSPE, the increased initial viscosity and chain entanglement before crosslinking significantly improve the processability of the SPE, which enables ~20 μm SPE fabrication.

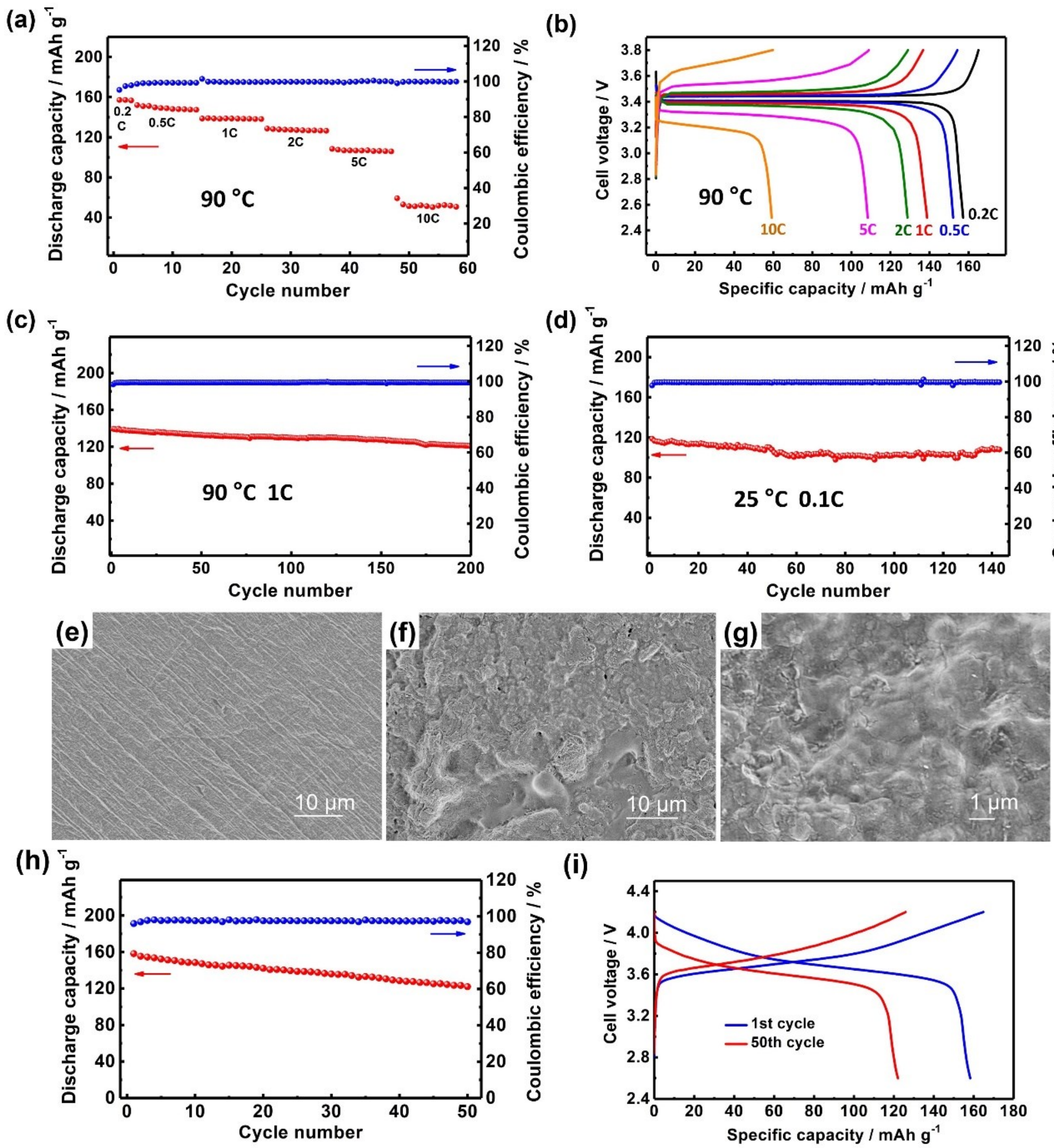

Figure 4. Full battery performance of ConSPE-based full cells. (a-g) Li/$LiFePO_4$ battery performance for the 4PGMA-PEG6k ConSPE: (a) discharge capacity and CE, and (b) charge-discharge curves under different current rates at 90 °C; (c) discharge capacity and CE at 90 °C under a 1 C rate; (d) discharge capacity and CE at 25 °C under a 0.1 C rate; SEM images of lithium anode surface (e) before and (f-g) after rate tests at 90 °C. (h-i) Li/$LiNi_{0.6}Mn_{0.2}Co_{0.2}O_2$ battery performance of 4PGMA-PEG6k ConSPE at 90 °C under a current density of 20 mA g^{-1}: (h) discharge capacity and CE, (i) charge-discharge curves for the 1st and 50th cycles.

$Li/LiFePO_4$ batteries were assembled using the ultra-thin 4PGMA-PEG6k ConSPE sample and cycled at different temperatures. **Figures 4a,b** show the battery performance at 90 °C under different current rates. The battery can deliver successful cycling even when the current rate reaches up to 10 C, and the discharge capacity reaches about 157, 152, 139, 129, 108 and 59 mAh g^{-1} under the current rates of 0.2 C, 0.5 C, 1 C, 2 C, 5 C, and 10 C, respectively, with stable cycling for each current rate. The discharge voltage plateau located at 3.4, 3.4, 3.38, 3.37, 3.3, and 3.18 V vs. Li/Li^+, exhibiting typical characteristics of $Li/LiFePO_4$ battery.[32, 53, 54] When cycled under a 1 C rate, the battery delivers stable discharge capacity with a capacity retention of 86.4% after 200 cycles (**Figure 4c**), and the average Coulombic efficiency (CE) is 99.5%, revealing remarkable stability of the battery system. The discharge capacities for the battery at 50 °C are 138, 119, and 108 mAh g^{-1} under 0.2 C, 0.5 C, and 1 C (**Figure S8**), and remain stable in the continuous cycling. Moreover, the ultra-thin ConSPE membrane enables successful cycling at a low temperature of 25 °C, with a discharge capacity of about 120 mAh g^{-1} at 0.1 C rate, and capacity retention of 92.2% after 140 cycles. SEM images of lithium anode surface after cycling at 90 °C (**Figures 4e-g**) show a compact nodular morphology without the presence of lithium dendrites, confirming the excellent lithium dendrite resistance of ConSPEs. Compared with previously reported SPEs,[18, 30, 46, 55-57] the ConSPE developed in this work delivers comparable or better performance at 90 °C, and the discharge capacity for the ConSPE at 50 °C is even higher than the reported data obtained at 60 °C.

Owing to the excellent anodic stability of 5.3 V vs. Li/Li^+, the PGMA-PEG ConSPE can also achieve stable cycling for LMBs using high-voltage $LiNi_{0.6}Mn_{0.2}Co_{0.2}O_2$ cathode[58-60] (**Figures 4h-i**). The $Li/LiNi_{0.6}Mn_{0.2}Co_{0.2}O_2$ battery with the 4PGMA-PEG6k ConSPE exhibits an initial discharge capacity of about 160 mAh g^{-1} at 90 °C under the current density of 20 mA g^{-1}, with a capacity retention close to 80% after 50 cycles, showing that the prepared PGMA-PEG ConSPEs have great potential for high-energy-density LMBs.

In summary, in this work, a series of solid polymer electrolytes were prepared using comb-chain PGMA as the cross-linker. The novel nanoscale network structure dramatically improves the network mechanical properties, which is demonstrated to be critical to lithium dendrite resistance. The ConSPEs show an impressively high ionic conductivity of 1.31×10^{-4} S cm^{-1} at 40 °C with excellent thermal stability and anodic stability. Li/$LiFePO_4$ batteries with the ConSPE deliver high discharge capacity and good cycling performance up to 10 C rate. The battery also allows stable cycling at 25 °C. In addition, stable cycling could be achieved for Li/$LiNi_{0.6}Mn_{0.2}Co_{0.2}O_2$ batteries with the ConSPE, exhibiting the great potential for the ConSPE in high-energy-density LMBs. These remarkable results reveal that the newly developed PGMA-PEG ConSPE is a promising electrolyte system for high-performance and dendrite-free LMBs.

ASSOCIATED CONTENT

Supporting Information

The following files are available free of charge.

Experimental section, Figures S1-S8, and Tables S1-S2 (PDF)

AUTHOR INFORMATION

Corresponding Author

*Christopher Y. Li – Department of Materials Science and Engineering, Drexel University, Philadelphia, PA 19104, USA; E-mail: chrisli@drexel.edu

Author Contributions

The manuscript was written through contributions of all authors. All authors have given approval to the final version of the manuscript.

Notes

The authors declare no competing financial interest.

ACKNOWLEDGMENT

We are grateful for the support from the National Science Foundation through grants CBET 1603520and CBET 2033882.

REFERENCES

(1) Armand, M.; Tarascon, J. M., Building better batteries. *Nature* **2008,** *451* (7179), 652-657.

(2) Tikekar, M. D.; Choudhury, S.; Tu, Z.; Archer, L. A., Design Principles for Electrolytes and Interfaces for Stable Lithium-Metal Batteries. *Nat. Energy* **2016,** *1* (9), 16114.

(3) Lin, D.; Liu, Y.; Cui, Y., Reviving the Lithium Metal Anode for High-Energy Batteries. *Nat. Nanotechnol.* **2017,** *12*, 194-206.

(4) Cheng, X.-B.; Zhang, R.; Zhao, C.-Z.; Zhang, Q., Toward Safe Lithium Metal Anode in Rechargeable Batteries: A Review. *Chem. Rev.* **2017,** *117* (15), 10403-10473.

(5) Liu, J.; Bao, Z.; Cui, Y.; Dufek, E. J.; Goodenough, J. B.; Khalifah, P.; Li, Q.; Liaw, B. Y.; Liu, P.; Manthiram, A.; Meng, Y. S.; Subramanian, V. R.; Toney, M. F.; Viswanathan, V. V.; Whittingham, M. S.; Xiao, J.; Xu, W.; Yang, J.; Yang, X.-Q.; Zhang, J.-G., Pathways for practical high-energy long-cycling lithium metal batteries. *Nat. Energy* **2019,** *4* (3), 180-186.

(6) Zhao, Q.; Stalin, S.; Zhao, C.-Z.; Archer, L. A., Designing solid-state electrolytes for safe, energy-dense batteries. *Nat. Rev. Mater.* **2020,** *5* (3), 229-252.

(7) Choudhury, S.; Stalin, S.; Vu, D.; Warren, A.; Deng, Y.; Biswal, P.; Archer, L. A., Solid-state polymer electrolytes for high-performance lithium metal batteries. *Nat. Commun.* **2019,** *10* (1), 4398.

(8) Lopez, J.; Mackanic, D. G.; Cui, Y.; Bao, Z., Designing polymers for advanced battery chemistries. *Nat. Rev. Mater.* **2019,** *4* (5), 312-330.

(9) Fan, L.; Wei, S.; Li, S.; Li, Q.; Lu, Y., Recent Progress of the Solid-State Electrolytes for High-Energy Metal-Based Batteries. *Adv. Energy Mater.* **2018,** *8* (11), 1702657.

(10) Manthiram, A.; Yu, X.; Wang, S., Lithium battery chemistries enabled by solid-state electrolytes. *Nat. Rev. Mater.* **2017,** *2* (4), 16103.

(11) Li, X.; Cheng, S.; Zheng, Y.; Li, C. Y., Morphology control in semicrystalline solid polymer electrolytes for lithium batteries. *Mol. Syst. Des. Eng.* **2019,** *4* (4), 793-803.

(12) Armand, M., The history of polymer electrolytes. *Solid State Ionics* **1994,** *69* (3), 309-319.

(13) Hallinan, D. T.; Balsara, N. P., Polymer Electrolytes. *Annu. Rev. Mater. Res.* **2013,** *43* (1), 503-525.

(14) Choo, Y.; Halat, D. M.; Villaluenga, I.; Timachova, K.; Balsara, N. P., Diffusion and migration in polymer electrolytes. *Prog. Polym. Sci.* **2020,** *103*, 101220.

(15) Young, W.-S.; Kuan, W.-F.; Epps, I. I. I. T. H., Block copolymer electrolytes for rechargeable lithium batteries. *J. Polym. Sci., Part B: Polym. Phys.* **2014,** *52* (1), 1-16.

(16) Cheng, S.; Smith, D. M.; Li, C. Y., How Does Nanoscale Crystalline Structure Affect Ion Transport in Solid Polymer Electrolytes? *Macromolecules* **2014,** *47* (12), 3978-3986.

(17) Cheng, S.; Smith, D. M.; Pan, Q.; Wang, S.; Li, C. Y., Anisotropic ion transport in nanostructured solid polymer electrolytes. *RSC Adv.* **2015,** *5* (60), 48793-48810.

(18) Pan, Q.; Smith, D. M.; Qi, H.; Wang, S.; Li, C. Y., Hybrid Electrolytes with Controlled Network Structures for Lithium Metal Batteries. *Adv. Mater.* **2015,** *27* (39), 5995-6001.

(19) Cao, C.; Li, Y.; Feng, Y.; Peng, C.; Li, Z.; Feng, W., A solid-state single-ion polymer electrolyte with ultrahigh ionic conductivity for dendrite-free lithium metal batteries. *Energy Storage Mater.* **2019,** *19*, 401-407.

(20) Huang, W.; Pan, Q.; Qi, H.; Li, X.; Tu, Y.; Li, C. Y., Poly(butylene terephthalate)-*b*-Poly(ethylene oxide) Alternating Multiblock Copolymers: Synthesis and Application in Solid Polymer Electrolytes. *Polymer* **2017,** *128*, 188-199.

(21) Smith, D. M.; Dong, B.; Marron, R. W.; Birnkrant, M. J.; Elabd, Y. A.; Natarajan, L. V.; Tondiglia, V. P.; Bunning, T. J.; Li, C. Y., Tuning Ion Conducting Pathways Using Holographic Polymerization. *Nano Lett.* **2012,** *12* (1), 310-314.

(22) Smith, D. M.; Pan, Q.; Cheng, S.; Wang, W.; Bunning, T. J.; Li, C. Y., Nanostructured, Highly Anisotropic, and Mechanically Robust Polymer Electrolyte Membranes via Holographic Polymerization. *Adv. Mater. Interfaces* **2018,** *5* (1), 1700861.

(23) Choudhury, S.; Mangal, R.; Agrawal, A.; Archer, L. A., A Highly Reversible Room-Temperature Lithium Metal Battery Based on Crosslinked Hairy Nanoparticles. *Nat. Commun.* **2015,** *6*, 10101.

(24) Khurana, R.; Schaefer, J. L.; Archer, L. A.; Coates, G. W., Suppression of Lithium Dendrite Growth Using Cross-Linked Polyethylene/Poly(ethylene oxide) Electrolytes: A New Approach for Practical Lithium-Metal Polymer Batteries. *J. Am. Chem. Soc.* **2014,** *136* (20), 7395-7402.

(25) Mackanic, D. G.; Michaels, W.; Lee, M.; Feng, D.; Lopez, J.; Qin, J.; Cui, Y.; Bao, Z., Crosslinked Poly(tetrahydrofuran) as a Loosely Coordinating Polymer Electrolyte. *Adv. Energy Mater.* **2018,** *8* (25), 1800703.

(26) Gu, Y.; Zhao, J.; Johnson, J. A., Polymer Networks: From Plastics and Gels to Porous Frameworks. *Angew. Chem. Int. Ed.* **2020,** *59* (13), 5022-5049.

(27) Odian, G., *Principles of Polymerization*, 4th ed.; John Wiley & Sons: Hoboken, NJ, 2004.

(28) Snyder, J. F.; Carter, R. H.; Wetzel, E. D., Electrochemical and Mechanical Behavior in Mechanically Robust Solid Polymer Electrolytes for Use in Multifunctional Structural Batteries. *Chem. Mater.* **2007,** *19* (15), 3793-3801.

(29) Zheng, Y.; Pan, Q.; Clites, M.; Byles, B. W.; Pomerantseva, E.; Li, C. Y., High-Capacity All-Solid-State Sodium Metal Battery with Hybrid Polymer Electrolytes. *Adv. Energy Mater.* **2018,** *8* (27), 1801885.

(30) Li, X.; Zheng, Y.; Pan, Q.; Li, C. Y., Polymerized Ionic Liquid-Containing Interpenetrating Network Solid Polymer Electrolytes for All-Solid-State Lithium Metal Batteries. *ACS Appl. Mater. Interfaces* **2019,** *11* (38), 34904-34912.

(31) Zheng, Y.; Li, X.; Li, C. Y., A novel de-coupling solid polymer electrolyte via semi-interpenetrating network for lithium metal battery. *Energy Storage Mater.* **2020,** *29*, 42-51.

(32) Huang, Z.; Pan, Q.; Smith, D. M.; Li, C. Y., Plasticized Hybrid Network Solid Polymer Electrolytes for Lithium-Metal Batteries. *Adv. Mater. Interfaces* **2019,** *6* (2), 1801445.

(33) Wunderlich, B., *Thermal Analysis of Polymeric Materials*. Springer Science & Business Media: 2005.

(34) Doughty, D. H.; Roth, E. P., A General Discussion of Li Ion Battery Safety. *Electrochem. Soc. Interface* **2012,** *21* (2), 37-44.

(35) Nugent, J. L.; Moganty, S. S.; Archer, L. A., Nanoscale Organic Hybrid Electrolytes. *Adv. Mater.* **2010,** *22* (33), 3677-3680.

(36) Lu, Y.; Das, S. K.; Moganty, S. S.; Archer, L. A., Ionic Liquid-Nanoparticle Hybrid Electrolytes and their Application in Secondary Lithium-Metal Batteries. *Adv. Mater.* **2012,** *24* (32), 4430-4435.

(37) Zhao, C.-Z.; Zhang, X.-Q.; Cheng, X.-B.; Zhang, R.; Xu, R.; Chen, P.-Y.; Peng, H.-J.; Huang, J.-Q.; Zhang, Q., An anion-immobilized composite electrolyte for dendrite-free lithium metal anodes. *Proc. Natl. Acad. Sci.* **2017,** *114* (42), 11069-11074.

(38) Sheng, O.; Jin, C.; Luo, J.; Yuan, H.; Huang, H.; Gan, Y.; Zhang, J.; Xia, Y.; Liang, C.; Zhang, W.; Tao, X., Mg2B2O5 Nanowire Enabled Multifunctional Solid-State Electrolytes with High Ionic Conductivity, Excellent Mechanical Properties, and Flame-Retardant Performance. *Nano Lett.* **2018,** *18* (5), 3104-3112.

(39) Mackanic, D. G.; Yan, X.; Zhang, Q.; Matsuhisa, N.; Yu, Z.; Jiang, Y.; Manika, T.; Lopez, J.; Yan, H.; Liu, K.; Chen, X.; Cui, Y.; Bao, Z., Decoupling of mechanical properties and ionic conductivity in supramolecular lithium ion conductors. *Nat. Commun.* **2019,** *10* (1), 5384.

(40) Xu, K., Electrolytes and Interphases in Li-Ion Batteries and Beyond. *Chem. Rev.* **2014,** *114* (23), 11503-11618.

(41) Chen, P.; Liu, X.; Wang, S.; Zeng, Q.; Wang, Z.; Li, Z.; Zhang, L., Confining Hyperbranched Star Poly(ethylene oxide)-Based Polymer into a 3D Interpenetrating Network for a High-Performance All-Solid-State Polymer Electrolyte. *ACS Appl. Mater. Interfaces* **2019,** *11* (46), 43146-43155.

(42) Yang, X.; Jiang, M.; Gao, X.; Bao, D.; Sun, Q.; Holmes, N.; Duan, H.; Mukherjee, S.; Adair, K.; Zhao, C.; Liang, J.; Li, W.; Li, J.; Liu, Y.; Huang, H.; Zhang, L.; Lu, S.; Lu, Q.; Li, R.; Singh, C. V.; Sun, X., Determining the limiting factor of the electrochemical stability window for PEO-based solid polymer electrolytes: main chain or terminal –OH group? *Energy Environ. Sci.* **2020,** *13* (5), 1318-1325.

(43) Gray, F. M.; Gray, F. M., *Solid polymer electrolytes: fundamentals and technological applications*. VCH New York: 1991.

(44) Monroe, C.; Newman, J., The Impact of Elastic Deformation on Deposition Kinetics at Lithium/Polymer Interfaces. *J. Electrochem. Soc.* **2005,** *152* (2), A396-A404.

(45) Hallinan, D. T.; Mullin, S. A.; Stone, G. M.; Balsara, N. P., Lithium Metal Stability in Batteries with Block Copolymer Electrolytes. *J. Electrochem. Soc.* **2013,** *160* (3), A464-A470.

(46) Pan, Q.; Barbash, D.; Smith, D. M.; Qi, H.; Gleeson, S. E.; Li, C. Y., Correlating Electrode–Electrolyte Interface and Battery Performance in Hybrid Solid Polymer Electrolyte-Based Lithium Metal Batteries. *Adv. Energy Mater.* **2017,** *7* (22), 1701231.

(47) Liu, S.; Imanishi, N.; Zhang, T.; Hirano, A.; Takeda, Y.; Yamamoto, O.; Yang, J., Effect of Nano-Silica Filler in Polymer Electrolyte on Li Dendrite Formation in Li/Poly(ethylene oxide)–$Li(CF_3SO_2)_2N$/Li. *J. Power Sources* **2010,** *195* (19), 6847-6853.

(48) Stone, G. M.; Mullin, S. A.; Teran, A. A.; Hallinan, D. T.; Minor, A. M.; Hexemer, A.; Balsara, N. P., Resolution of the Modulus versus Adhesion Dilemma in Solid Polymer Electrolytes for Rechargeable Lithium Metal Batteries. *J. Electrochem. Soc.* **2012,** *159* (3), A222-A227.

(49) Zheng, Q.; Ma, L.; Khurana, R.; Archer, L. A.; Coates, G. W., Structure–Property Study of Cross-Linked Hydrocarbon/Poly(ethylene oxide) Electrolytes with Superior Conductivity and Dendrite Resistance. *Chem. Sci.* **2016,** *7* (11), 6832-6838.

(50) Xu, C.; Sun, B.; Gustafsson, T.; Edström, K.; Brandell, D.; Hahlin, M., Interface layer formation in solid polymer electrolyte lithium batteries: an XPS study. *J. Mater. Chem. A* **2014,** *2* (20), 7256-7264.

(51) Peled, E., Advanced Model for Solid Electrolyte Interphase Electrodes in Liquid and Polymer Electrolytes. *J. Electrochem. Soc.* **1997,** *144* (8), L208.

(52) Wan, J.; Xie, J.; Kong, X.; Liu, Z.; Liu, K.; Shi, F.; Pei, A.; Chen, H.; Chen, W.; Chen, J.; Zhang, X.; Zong, L.; Wang, J.; Chen, L.-Q.; Qin, J.; Cui, Y., Ultrathin, flexible, solid polymer composite electrolyte enabled with aligned nanoporous host for lithium batteries. *Nat. Nanotechnol.* **2019,** *14* (7), 705-711.

(53) Li, X.; Li, S.; Zhang, Z.; Huang, J.; Yang, L.; Hirano, S.-i., High-Performance Polymeric Ionic Liquid-Silica Hybrid Ionogel Electrolytes for Lithium Metal Batteries. *J. Mater. Chem. A* **2016,** *4* (36), 13822-13829.

(54) Li, X.; Zhang, Z.; Li, S.; Yang, K.; Yang, L., Polymeric Ionic Liquid-Ionic Plastic Crystal All-Solid-State Electrolytes for Wide Operating Temperature Range Lithium Metal Batteries. *J. Mater. Chem. A* **2017,** *5* (40), 21362-21369.

(55) Wang, L.; Li, X.; Yang, W., Enhancement of electrochemical properties of hot-pressed poly(ethylene oxide)-based nanocomposite polymer electrolyte films for all-solid-state lithium polymer batteries. *Electrochim. Acta* **2010,** *55* (6), 1895-1899.

(56) Chen, Y.; Shi, Y.; Liang, Y.; Dong, H.; Hao, F.; Wang, A.; Zhu, Y.; Cui, X.; Yao, Y., Hyperbranched PEO-Based Hyperstar Solid Polymer Electrolytes with Simultaneous Improvement of Ion Transport and Mechanical Strength. *ACS Appl. Energy Mater.* **2019,** *2* (3), 1608-1615.

(57) Hu, J.; Wang, W.; Peng, H.; Guo, M.; Feng, Y.; Xue, Z.; Ye, Y.; Xie, X., Flexible Organic–Inorganic Hybrid Solid Electrolytes Formed via Thiol–Acrylate Photopolymerization. *Macromolecules* **2017,** *50* (5), 1970-1980.

(58) Zhang, H.; Zhang, J.; Ma, J.; Xu, G.; Dong, T.; Cui, G., Polymer Electrolytes for High Energy Density Ternary Cathode Material-Based Lithium Batteries. *Electrochem. Energ. Rev.* **2019,** *2* (1), 128-148.

(59) Li, Z.; Xie, H.-X.; Zhang, X.-Y.; Guo, X., In situ thermally polymerized solid composite electrolytes with a broad electrochemical window for all-solid-state lithium metal batteries. *J. Mater. Chem. A* **2020,** *8* (7), 3892-3900.

(60) Li, X.; Zheng, Y.; Li, C. Y., Dendrite-free, wide temperature range lithium metal batteries enabled by hybrid network ionic liquids. *Energy Storage Mater.* **2020,** *29*, 273-280.

For Table of Contents Only